The Astronomical Journal, 162:284 (9pp), 2021 December https://doi.org/10.3847/1538-3881/ac178a

The Posttransit Tail of WASP-107b Observed at 10830 Å

J. J. Spake[1], A. Oklopčić[2], and L. A. Hillenbrand[3]
[1] Division of Geological and Planetary Sciences, California Institute of Technology, Pasadena, CA 91125, USA; jessica.spake@gmail.com
[2] Anton Pannekoek Institute of Astronomy, University of Amsterdam, Science Park 904, 1098 XH Amsterdam, Netherlands
[3] Department of Astronomy, California Institute of Technology, Pasadena, CA 91125, USA
Received 2021 March 23; revised 2021 July 19; accepted 2021 July 22; published 2021 December 2

Abstract

Understanding the effects of high-energy radiation and stellar winds on planetary atmospheres is vital for explaining the observed properties of close-in exoplanets. Observations of transiting exoplanets in the triplet of metastable helium lines at 10830 Å allow extended atmospheres and escape processes to be studied for individual planets. We observed one transit of WASP-107b with NIRSPEC on Keck at 10830 Å. Our observations, for the first time, had significant posttransit phase coverage, and we detected excess absorption for over an hour after fourth contact. The data can be explained by a comet-like tail extending out to ∼7 planet radii, which corresponds to roughly twice the Roche lobe radius of the planet. Planetary tails are expected based on three-dimensional simulations of escaping exoplanet atmospheres, particularly those including the interaction between the escaped material and strong stellar winds, and have been previously observed at 10830 Å in at least one other exoplanet. With both the largest midtransit absorption signal and the most extended tail observed at 10830 Å, WASP-107b remains a keystone exoplanet for atmospheric escape studies.

Unified Astronomy Thesaurus concepts: Exoplanets (498); Exoplanet astronomy (486); Extrasolar gaseous planets (2172); Exoplanet atmospheres (487); Exoplanet atmospheric composition (2021)

1. Introduction

Most known transiting exoplanets orbit close to their host stars and are therefore highly irradiated, which makes them likely susceptible to atmospheric escape. Population studies of bulk properties, like planet radius and orbital distance, can illuminate how mass-loss change compositions and radii over planetary lifetimes, especially for the more numerous, smaller exoplanets (e.g., Lopez & Fortney 2013; Owen & Wu 2013; Fulton et al. 2017; Ginzburg et al. 2018). On the other hand, individual, gas-rich exoplanets on close orbits around bright stars are amenable to atmospheric characterization, and therefore allow atmospheric escape to be seen in action.

Transmission spectroscopy is a powerful method for probing exoplanet atmospheres (e.g., Seager & Sasselov 2000). Strong absorption lines of species that are abundant at high altitudes, where gas is rarefied, are the most useful for observing atmospheric escape. For example, the Lyα line of ground-state hydrogen was the first absorption line used to find exoplanet atmospheres overflowing their Roche radii, for the hot-Jupiters HD209458b (Vidal-Madjar et al. 2003) and HD189733b (Lecavelier Des Etangs et al. 2010). The Hα line, from the first excited state of hydrogen, has also been used to observe the high-altitude thermospheres of exoplanets, where mass loss is thought to be launched (e.g., Jensen et al. 2012; Yan & Henning 2018). Heavier, but still abundant elements, like carbon, oxygen, magnesium, and iron, have also been observed overflowing (or close to) the Roche radii of some planets (e.g., Vidal-Madjar et al. 2004, 2013; Sing et al. 2019).

The Lyα observations were also the first to directly demonstrate "tails" of lost material trailing behind exoplanets, which manifest as posttransit absorption in the observed light curves. The most dramatic example of a planetary tail is that of the hot Neptune GJ436b (Kulow et al. 2014; Ehrenreich et al. 2015; Lavie et al. 2017), which blocks $56.3\% \pm 3.5\%$ of the stellar radiation at midtransit, and shows blueshifted absorption over three hours after the end of the nominal one-hour transit, at radial velocities up to $-100\,\mathrm{km\,s^{-1}}$. The absorption also begins two hours before the nominal ingress. Combined, these observations imply an asymmetric cloud of material surrounding the planet, with a trailing tail shaped by stellar wind that is longer than the planet's radial distance to the star (Ehrenreich et al. 2015). For the hot-Jupiter HD189733b, excess absorption was observed for at least 30 minutes posttransit in just one of the five observed Lyα light curves, which happened to occur 8 hr after a stellar flare (Lecavelier Des Etangs et al. 2010, 2012). The result indicated variability in the escaping planetary wind, possibly caused by the varying stellar environment. For HD 209458b, which is less massive than HD189733b, strong absorption was seen at egress with high-resolution Lyα observations, which indicated a comet-like tail. However, the observations did not have the posttransit coverage needed to observe it directly (Vidal-Madjar et al. 2003). Planetary tails have long been predicted (e.g., Schneider et al. 1998) and studied in a number of three-dimensional (3D) numerical simulations of atmospheric escape in exoplanets (e.g., Bisikalo et al. 2013; Matsakos et al. 2015; Bourrier et al. 2016; Christie et al. 2016; Carroll-Nellenback et al. 2017; Khodachenko et al. 2019; McCann et al. 2019; Carolan et al. 2021).

Pretransit absorption has been observed in several planets, including the aforementioned GJ 436b. Fossati et al. (2010) detected an early ingress for the hot-Jupiter WASP-12b in a broadband light curve at NUV wavelengths. For HD189733b, evidence of pretransit absorption has been observed in absorption lines of three separate species: Fossati et al. (2010) detected absorption by C II in two separate transit events; Bourrier et al. (2013) detected absorption by Si III; and Cauley et al. (2015, 2016) detected absorption in Hα. These observations have been explained by models of a bow shock at the interface of the planetary and stellar wind, although it is unclear how much stellar variability contributes to the signal,

Table 1
Adopted System Parameters for WASP-107b

Param.	Unit	Value	Source
P	day	5.7214742	Dai & Winn (2017)
t_c	JD	2458494.04427	Dai & Winn (2017)
b		0.07 ± 0.07	Dai & Winn (2017)
i	°	$89.887^{+0.074}_{-0.097}$	Dai & Winn (2017)
R_p/R_*		0.14434 ± 0.00018	Dai & Winn (2017)
a/R_*		18.164 ± 0.037	Dai & Winn (2017)
M_P	M_J	0.096 ± 0.005	Piaulet et al. (2021)
e		0.06 ± 0.04	Piaulet et al. (2021)
ω	°	40^{+40}_{-60}	Piaulet et al. (2021)
$T_{\rm eff}$	K	4245 ± 70	Piaulet et al. (2021)
M_*	$M_\odot$	$0.683^{+0.017}_{-0.016}$	Piaulet et al. (2021)
R_*	$R_\odot$	0.67 ± 0.02	Piaulet et al. (2021)

especially as the signal size seems to correlate with stellar activity levels (e.g., Cauley et al. 2016).

In recent years, the neutral helium line triplet at 10830 Å[4] has been established as a new probe of extended and escaping exoplanet atmospheres (Seager & Sasselov 2000; Oklopčić & Hirata 2018). Spake et al. (2018) first observed helium in the extended atmosphere of the inflated sub-Saturn orbiting a K6 star, WASP-107b, at 10830 Å, with low-resolution spectra from the Hubble Space Telescope (HST)/Wide Field Camera 3. Since then there have been numerous observations of extended and escaping exoplanet atmospheres using the 10830 Å lines (e.g., Allart et al. 2018; Mansfield et al. 2018; Nortmann et al. 2018; Salz et al. 2018; Alonso-Floriano et al. 2019; Ninan et al. 2020; Palle et al. 2020; Vissapragada et al. 2020; Paragas et al. 2021), and notable nondetections, only some of which have been published (e.g., Kasper et al. 2020; Zhang et al. 2021). Of particular relevance to this work, Nortmann et al. (2018) used CARMENES (Quirrenbach et al. 2014) to observe the 10830 Å transmission spectrum of WASP-69b—a warm, inflated, Saturn-mass exoplanet orbiting a K5 star. They reported significant posttransit absorption, indicative of a planetary tail that extended slightly further than the planet's Roche radius.

WASP-107b, which was discovered by Anderson et al. (2017), remains the exoplanet with the strongest helium signal observed so far. Additionally, its retrograde, polar orbit (Rubenzahl et al. 2021), extremely low density ($0.13^{+0.015}_{-0.013}$ g cm^{-3}), and distant companion (planet c; Piaulet et al. 2021) have furthered interest in this unusual planet. Table 1 lists the stellar and planetary parameters adopted in this study of planet b. The low-resolution HST helium detection was confirmed by Allart et al. (2019), who measured excess helium absorption of $5.54\% \pm 0.27\%$ in the core of the deepest component of the lines, using high-resolution data obtained with the ground-based CARMENES spectrograph. The signal is large compared to the $\sim$2% transit depth of the planet at broadband optical wavelengths (Anderson et al. 2017). Kirk et al. (2020) re-observed WASP-107b at high resolution with NIRSPEC on Keck, and found a transmission spectrum consistent with the CARMENES observations. They additionally noted excess absorption during the planet's egress, hinting at the presence of a comet-like tail.

[4] All absorption lines listed in this paper are at air wavelengths.

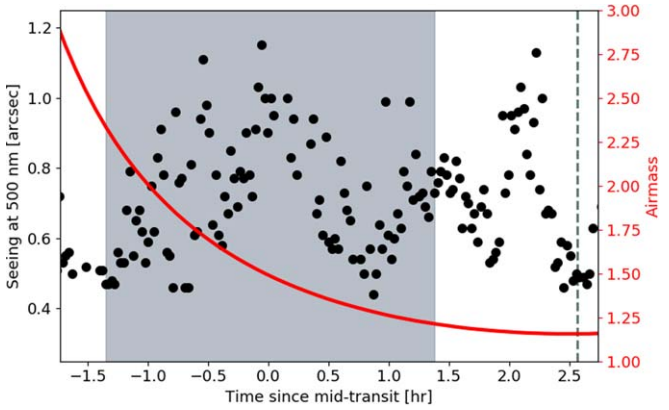

Figure 1. Seeing (black dots) and airmass (red line) during our 2019 January observations. Seeing data were obtained from the Maunakea Weather Center. The duration of the broadband transit is shown in gray. Dashed vertical line marks the 18° dawn.

Hydrodynamic simulations, similar to those developed for predicting the observable signatures of atmospheric escape and planetary tails in the Lyα line, can be used to produce synthetic spectra in the He 10830 Å lines (e.g., Wang & Dai 2021a, 2021b; M. MacLeod & A. Oklopčić 2021, in preparation; Shaikhislamov et al. 2021). Recently, Wang & Dai (2021b) simulated the 10830 Å observations of WASP-107b, and their fiducial model suggests the presence of a comet-like tail of material trailing behind the planet. The tail would manifest as an asymmetric transit light curve at 10830 Å, with a prolonged absorption after the fourth transit contact. Wang & Dai (2021b) noted a hint of asymmetry in the NIRSPEC light curve based on the data originally presented by Kirk et al. (2020). However, neither Allart et al. (2019) nor Kirk et al. (2020) observed WASP-107b with significant postegress phase coverage, so they were unlikely to directly detect a tail.

Here we present a new transit observation of WASP-107b at high resolution around 10830 Å, with NIRSPEC on Keck. Our data were taken between the two transits studied in Allart et al. (2019) and Kirk et al. (2020). We observed over an hour's worth of high-resolution spectra after the nominal planet egress, and as a result, for the first time directly detected excess helium absorption from a comet-like tail of material lost from the planet.

2. Observations

To observe a transit of WASP-107b, we used the newly-upgraded (Martin et al. 2018) NIRSPEC spectrograph (McLean et al. 1998, 2000) on the 10 m Keck II telescope, for one half night. Observations were performed using NIRSPEC in its echelle mode with the N1 (Y-band) filter, having effective wavelength coverage from 0.941–1.122 μm, with some overlap and no gaps between the orders. The helium triplet lines appear in both Order 70 and Order 71, at rest wavelengths of 10830.34, 10830.25, and 10829.09 Å. In this work we only present data from order 70. We used the $0\farcs288 \times 12''$ slit, resulting in spectral resolution of $R = 37{,}000$ (corresponding to $\Delta v \approx 7.7$ km s^{-1}) at the wavelength of the helium line.

Our WASP-107b transit observations were performed on 2019 January 10 UT (program ID:C247, PI: Hillenbrand). The seeing was variable during the observations but averaged $\sim 0\farcs7$ (Figure 1). We used a standard ABBA nodding pattern with $4''$

throw between the nod positions and individual exposures of 300 s. Similarly to Kirk et al. (2020), we used the thin blocker, which introduces fringing in Y-band data. However, fringing effects are weak around 10830 Å, in order 70. Additionally, because our final results were produced by finding the difference between observed spectra, the effect of fringing was subtracted out. We did not observe any fringing pattern above the photon noise level in our final results.

We obtained a sequence of 48 individual spectra, with a S/N increasing from 55 to 80 per resolution element as the source rose in altitude. The first four spectra were taken with shorter exposures (60 s) compared to the rest of the sample (300 s), so we merged them and treated them as a single spectrum in the rest of the analysis. We discarded from our analysis two exposures (#32 and #42 in our sequence) taken while we were experiencing software issues, leaving 43 spectra which we used in our analysis.

On 2019 April 8 UT we observed WASP 107 at an orbital phase of 0.35 for planet b—well outside of transit. An additional set of four spectra were again obtained with NIRSPEC's N1 filter in the ABBA nod pattern, also with the $0\farcs288 \times 12''$ slit, but with exposure times of 180 s. Coincidentally, these extra observations occurred one night after the transit observation made by Kirk et al. (2020).

3. Data Reduction

First, to correct for bad pixels and cosmic rays, we applied the iterative bad pixel algorithm from REDSPEC (Kim et al. 2015), which we translated to Python, to every science exposure and flat field. We then made night-averaged flat fields by median combining eleven 5 second exposures of a halogen lamp, from which we subtracted the median of eleven 5 second exposures taken with the lamp off, to account for detector bias and dark current. To extract 1D spectra from the raw frames, we used a customized version of the NIRSPEC Data Reduction Pipeline[5] (NSDRP), which is written in Python. Before extraction, NSDRP performs flat-field correction, removal of telluric emission by pairwise subtraction of consecutive images, and spatial and spectral rectification of misaligned images. NSDRP had not yet been updated since NIRSPECs detector was upgraded, in late 2018, from an Aladdin III InSb 1024×1024 array to a Teledyne HAWAII-2RG HgCdTe 2048×2048 array. Therefore, we updated the hard-coded, expected positions of each spectral order on the detector to their new positions, and adapted the pipeline to handle 2048×2048 images rather than 1024×1024 images.

To determine the wavelength solution for each 1D spectrum on the night of 2019 January 19 ("January transit" hereafter), we followed a similar method to Zhang et al. (2021). First, we selected a model stellar spectrum from the PHOENIX grid appropriate for WASP-107 ($T_{\rm eff} = 4400$ K; $\log(g) = 4.5$; [M/H] = 0.0; Husser et al. 2013) to which we added a telluric transmission spectrum,[6] which had been shifted to account for the Earth's night-averaged radial velocity relative to the star. We then down sampled the resulting template spectrum to match the instrumental resolution ($R = 37{,}500$). We modeled the wavelength solution as a third-order Chebyshev polynomial (mathematically equivalent to monomials, but well behaved

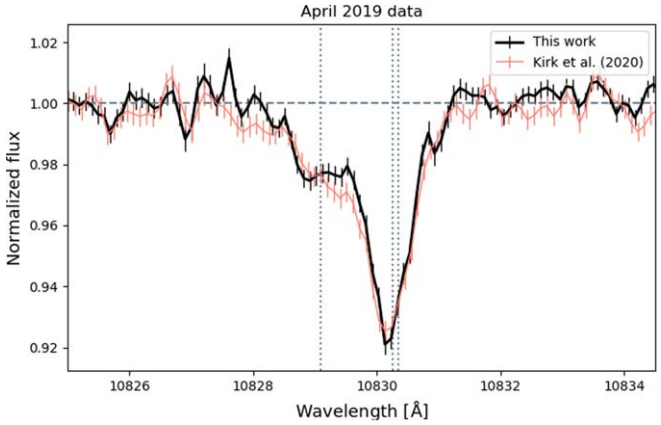

Figure 2. Excess absorption spectrum of WASP-107b (in the planet's frame) based on data obtained in 2019 April by Kirk et al. (2020). Wavelengths of the He I triplet indicated by dotted lines. The black line shows the result obtained using our data reduction, which agrees within observational uncertainty with the result presented in Kirk et al. (2020), shown in red.

around zero), and the stellar continuum as a fifth-order Chebyshev polynomial. We then used SCIPY's differential evolution to minimize the χ^2 between the continuum-normalized observations and the template spectrum. This method results in wavelength-calibrated, 1D spectra in the stellar rest frame, with line positions aligning with the model to better than one pixel.

To correct for telluric absorption lines, we used ESO's `molecfit` (Kausch et al. 2015; Smette et al. 2015). `molecfit` models telluric absorption at the observatory coordinates at a given time and airmass using Global Data Assimilation System[7] atmospheric profiles, which depend on local weather conditions. Before inputting the spectra, we shifted them from the stellar rest frame to the barycentric rest frame, and we shifted them back to the stellar rest frame after the `molecfit` correction. Similarly to Kirk et al. (2020), we isolated 10 telluric absorption lines across order 70, which did not overlap with strong stellar absorption lines and masked the rest of the spectra in each fit. Due to the combined systemic and barycentric radial velocities at the time of our observations, no strong telluric absorption lines overlapped with the helium 10830 Å triplet, as discussed in Section 4.3. For continuum normalization, we used iSpec (Blanco-Cuaresma et al. 2014) to find a polynomial fit to the extracted, telluric-corrected spectra, avoiding regions with strong stellar absorption lines (such as the region containing the He triplet and the nearby Si line).

To validate our reduction pipeline we also ran it on the previously published transit observation of WASP-107b using NIRSPEC in Y-band with a wider ($0\farcs433 \times 12''$) slit, taken on 2019 April 6, by Kirk et al. (2020; "April transit" hereafter). A comparison between the resulting transmission spectrum from the April transit using our pipeline, and that published by Kirk et al. (2020) is shown in Figure 2. For both reductions, the first six spectra were used to make the out-of-transit spectrum, and the 12 spectra between second and third contact (numbers 17–28 inclusive) were used to make the in-transit spectrum. The two independent reductions are consistent within the 1σ error bars. For the comparison of data sets obtained using different slit widths, discussed in Section 4.3, we used iSpec to

[5] https://github.com/Keck-DataReductionPipelines/NIRSPEC-Data-Reduction-Pipeline
[6] https://www.gemini.edu/observing/telescopes-and-sites/sites
[7] https://www.ncdc.noaa.gov/data-access/model-data/model-datasets/global-data-assimilation-system-gdas

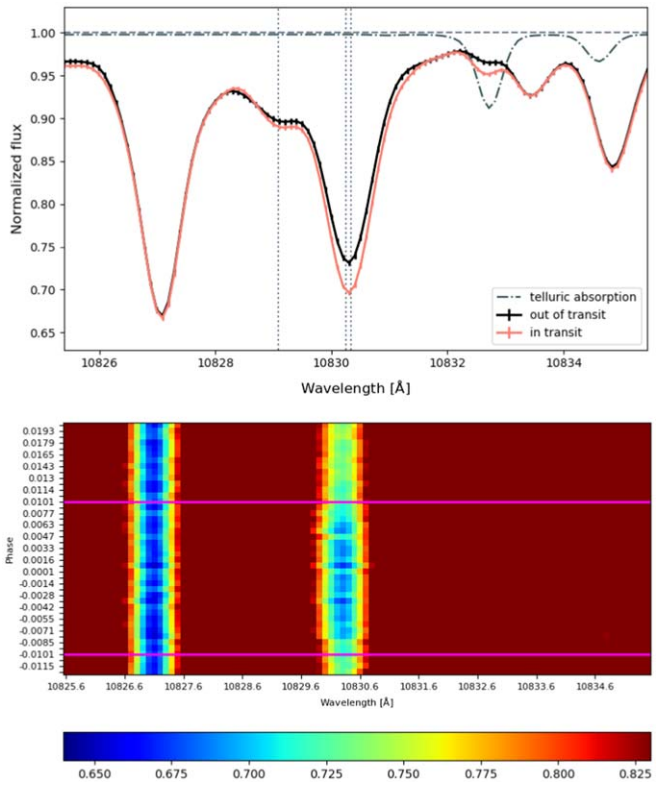

Figure 3. Top panel: in-transit and out-of-transit spectra of WASP-107, centered on the wavelengths of the He I triplet indicated by dotted lines. Excess absorption during the (broadband) transit of the planet is clearly noticeable. Bottom panel: orbital phase vs. wavelength map showing absorption depth in the He I line (the main component) and a nearby Si I line. The He I line depth increases between ingress and egress (magenta lines), while the Si I line stays constant.

first degrade the spectral resolution of all extracted spectra to $R = 25{,}000$, before combining them.

For the extra set of four spectra of WASP-107 taken on 2019 April 8 ("April 0.35 phase" hereafter), we used the same reduction method described above, and averaged the four spectra.

4. Results

4.1. January Absorption Spectrum

For the January transit data, we made a nominal transmission spectrum for WASP-107b, assuming the planet does not have a tail. To do this, we made an average "out-of-transit" spectrum, shown in Figure 3, using our 12 spectra taken after the fourth contact of the nominal planet transit (after the dashed line at phase 0.0104 in Figure 4). We then made an average in-transit spectrum (Figure 3) from our 21 spectra taken between second and third contacts of the nominal planet transit (between the dotted lines in Figure 4). The ratio between the average "in" and "out" spectra is shown in Figure 5. The excess absorption calculated this way is dramatically less than that reported by Kirk et al. (2020), and the peak also appears redshifted in comparison.

4.2. Excess Absorption Light Curves

We created an excess absorption light curve for the January transit. To do so, we first made individual excess absorption spectra by dividing each of the 43 normalized spectra by the

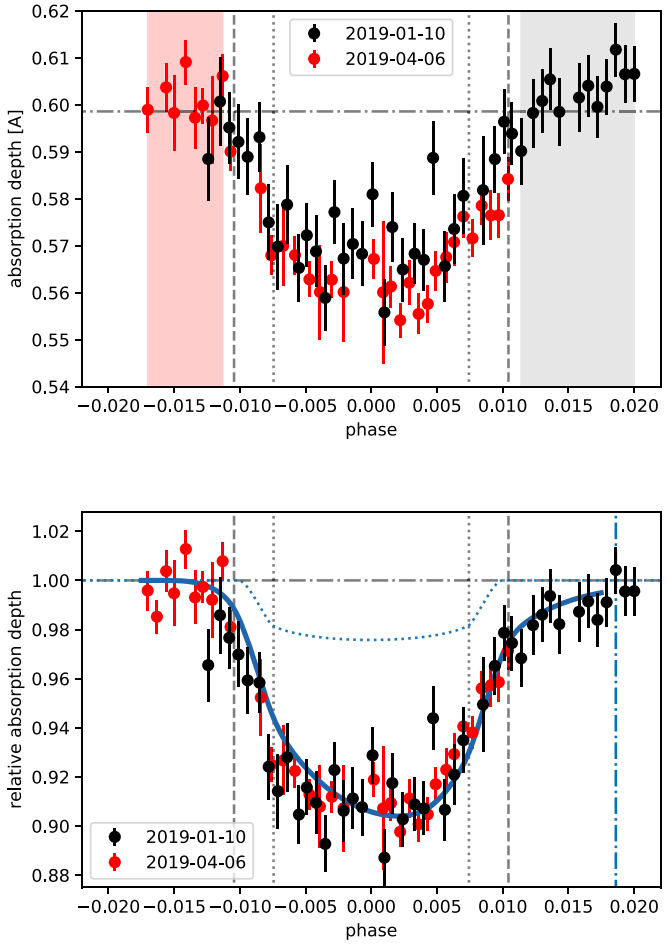

Figure 4. Top panel: light curves showing excess helium absorption integrated over wavelengths between 1082.983 and 1083.058 nm. The gray(red) area shows phases used for the construction of the out-of-transit spectrum for the January (April) night. Bottom panel: same as top panel, but both light curves are added to the white-light curve from Spake et al. (2018; dotted blue curve), and then normalized so that the transit depths match. Solid blue curve is the light curve based on the fiducial hydrodynamic simulation from Wang & Dai (2021b). Dashed–dotted vertical line indicates the end of the posttransit absorption.

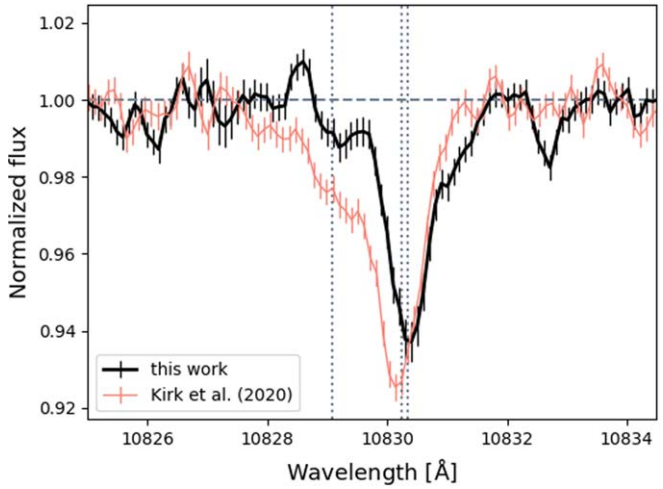

Figure 5. Absorption spectrum of WASP-107b, assuming no posttransit tail, in the reference frame of the planet observed in 2019 January (black). Wavelengths of the He I triplet indicated by dotted lines. The spectrum obtained by Kirk et al. (2020) using the same instrument in 2019 April is shown for comparison (red).

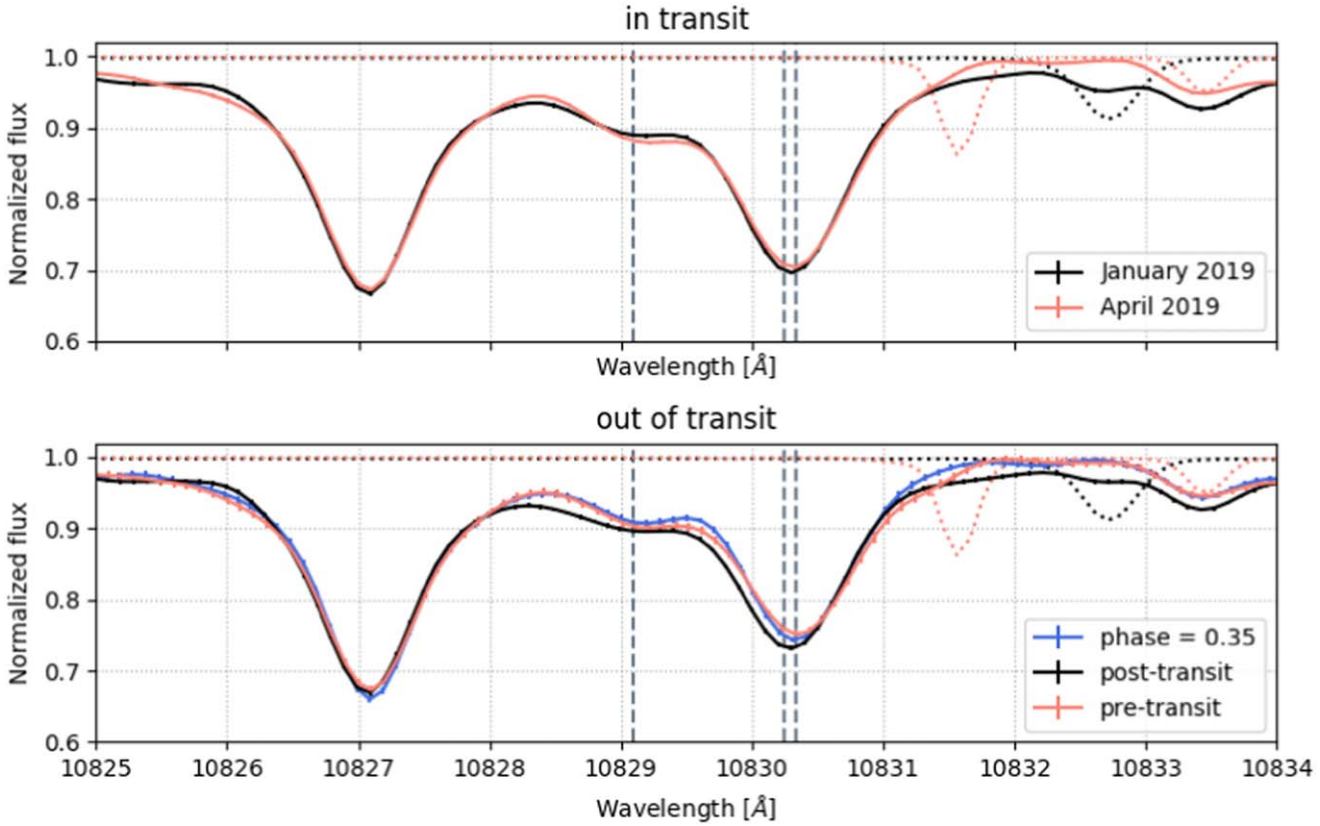

Figure 6. Comparison of in-transit and out-of-transit spectra of WASP-107 obtained with Keck/NIRSPEC in January (posttransit); 2019 April 6th (pretransit) and April 8th (phase = 0.35). 1σ errors are plotted as vertical bars, barely visible. For this comparison, the January and April 8th data have been degraded to spectral resolution of $R = 25{,}000$, same as the April 6th data. Dotted lines show the telluric absorption corrections for different data sets obtained using `molecfit`. Outside of the wavelength range contaminated by telluric lines, the largest difference is seen at the wavelengths of the He I triplet (vertical dashed lines) between the spectra observed shortly after transit (black lines) and the spectra observed either shortly before (red lines) or well after transit (blue line).

average "out-of-transit" spectrum shown in Figure 3. Then we integrated the flux between 10829.83 and 10830.58 Å for each of the excess absorption spectra, shown in Figure 4, top panel. We also show the light curve from our reduction of the April transit, calculated the same way, but using the first eight spectra in that data set to create an average out-of-transit spectrum. With this method, the January transit depth appears shallower than the April transit depth. Also, the posttransit absorption for the January transit continues to decrease well after transit, so that the light curve reaches a level higher than the pretransit observations at a phase of 0.02.

In the bottom panel of Figure 4, we also show the same two light curves, added to the broadband light curve covering 9000–10000 Å from Spake et al. (2018), and then normalized in such a way that the transit depths match. To do this, we calculated the weighted means of the two unnormalized light curves between the second and third contact points. We then subtracted the difference between the means from the January transit light curve. For normalization, we divided both light curves by the weighted mean of the pretransit April light curve (i.e., before first contact, dashed line at phase 0.0104 in Figure 4). The shape of the light curve is very consistent between the two observations when they are offset this way, being deeper after midtransit, and tapering off more slowly at egress than at ingress. Posttransit absorption is apparent in the January transit.

4.3. In versus Out Spectra

Figure 6 shows the averaged in-transit and "out-of-transit" spectra for the January transit, and the equivalent spectra from our reduction of the April transit. We stress that the January "out" spectrum (bottom panel) was made from data taken after the nominal planetary egress, but the "out" spectrum from the April transit was made from preingress data only. The "out" spectra from the two nights are noticeably different, especially in the blue wings of both components of the helium triplet, where there appears to be more absorption in the January data. On the other hand, the in-transit spectra (top panel) are much more similar between the two observations. The most significant difference in both the "in" and "out" spectra between the two nights occurs at wavelengths 10831.5–10834.0 Å. As we show in Figure 6, those wavelengths correspond to strong telluric absorption lines that we have corrected with `molecfit`, apparently imperfectly. Therefore we do not consider the difference at these wavelengths as astrophysical in origin, nor do we believe that telluric absorption has contaminated the helium 10830 Å line triplet.

4.4. April 0.35 Phase Data

Figure 6 (bottom panel) also shows the average of our four spectra taken one night after the April transit, at an orbital phase of 0.35. We can reasonably assume that this later spectrum is uncontaminated by transiting planetary material.

The April pretransit spectrum is much more similar to the April 0.35 phase spectrum than to the January posttransit spectrum. However, there are some slight differences: slightly more absorption in the pretransit data at 10829.7 and 10831 Å, but slightly less absorption in the core of the strongest component of the line, at 10830.3 Å.

4.5. Summary of Results

To summarize: we detected a transit of WASP-107b at 10830 Å, with an in-transit absorption spectrum (Figure 6, top panel) consistent with previously published results; we demonstrated asymmetry in the transit light curves; and we found evidence for blueshifted, posttransit absorption at 10830 Å.

5. Analysis

5.1. Possible Causes of Variation in He I 10830 Transmission Profiles

Here we discuss why our January transit data and the April transit data, originally published by Kirk et al. (2020), are different.

5.1.1. A Posttransit Tail

Because the in-transit spectra from the January and April transits are so similar (Figure 6, top panel), the difference between the planetary transmission spectra (Figure 5) must originate in the out-of-transit data (Figure 6, bottom panel). It is notable that our observations were taken in between the CARMENES transit presented by Allart et al. (2019), and the Keck transit by Kirk et al. (2020), which both had consistent absorption spectra, suggesting that the in-transit absorption profile is stable over months-long timescales within the instrumental precision.

We find that the most likely explanation for the deeper absorption and relative blueshift in the January "out" spectrum is contamination from a planetary tail streaming behind the planet. Hydrodynamic simulations of escaping planetary atmospheres generally predict that the escaped material should form a comet-like tail, further shaped by the interaction with the stellar wind. For WASP-107b specifically, the modeling work of Wang & Dai (2021b) shows that the evidence of a planetary tail should be observable in the He 10830 Å spectra.

5.1.2. Contrast Effect

The out-of-transit spectrum is set by the integrated stellar disk, but during a transit the planet blocks flux from the spatially resolved transit chord. Therefore, wavelength-dependent differences between the integrated stellar disk and the transit chord will appear in the transmission spectrum (e.g., Pont et al. 2008; Sing et al. 2011; McCullough et al. 2014). The effect of heterogeneous photospheres on exoplanet transmission spectra has been extensively modeled for FGKM stars (e.g., Cegla et al. 2018; Rackham et al. 2018, 2019). Cauley et al. (2018) did the same for chromospheric lines, including He 10830 Å, and concluded that it was difficult to create false-positive detections of 10830 Å in exoplanet atmospheres with the contrast effect.

However, stellar rotation combined with the oblique orbit of WASP-107b (Dai & Winn 2017; Rubenzahl et al. 2021) can result in the planet passing over different quiet or active regions of the star at different epochs. Therefore we could expect the contrast effect, and hence the measured transmission spectrum, to vary from visit to visit for this system. In principle, this could cause the variations we see in the January versus April WASP-107b transit spectra (Figure 5). Such visit-to-visit variations have been observed in 10830 Å transmission spectra of HD189733b by Guilluy et al. (2020), who analyzed five transits of the planet and saw changes in the transmission spectrum, which they attributed to the contrast effect. However, for HD189733b, there is strong evidence for spot- and faculae-crossing events in the time-series light curves from the visits that deviate from the average transmission spectrum. There is little evidence for similar spot or faculae-crossing events in the January transit light curve of WASP-107b at 10830 Å, and the shape of the January and April light curves presented here are remarkably similar when the transit depths are forced to match.

Finally, the contrast effect cannot explain why we see a significant difference in the "out-of-transit" spectrum, while the in-transit spectra look more similar (Figure 6).

5.1.3. Variability in the Planetary Wind

The midtransit absorption by the planet itself may vary from epoch to epoch—either due to a changing mass-loss rate or a changing population fraction of the excited 2^3S (metastable) state of helium, which is the origin of the 10830 Å absorption line. Such changes could be caused by varying extreme-ultraviolet flux from the star (e.g., Oklopčić 2019), which is dependent on the level of magnetic activity of the planet-facing hemisphere. For example, a higher stellar EUV flux during the April transit could lead to a greater midtransit absorption signal compared to that of the January transit (as seen in Figure 5). However, we might expect to see this in the out-of-transit data as increased stellar 10830 Å absorption, since the stellar EUV flux also populates the metastable state in the stellar chromosphere. In fact, the April out-of-transit 10830 Å absorption is weaker than that of January (assuming no planetary tail).

Several studies, including Wang & Dai (2021b) and McCann et al. (2019), have found that shear instabilities due to interaction with a stellar wind can change the level of absorption observed in transit light curves of escaping atmospheres. The greatest variability is seen in the pre and posttransit absorption; however, they also report low levels of variability between second and third contact. For the fiducial model of Wang & Dai (2021b), which best fits the observations of Allart et al. (2019) and Kirk et al. (2020), the midtransit variations are small, totaling less than 5% of the equivalent width of the absorption line. The consistency of the Allart et al. (2019) and Kirk et al. (2020) transmission spectra, which sandwiched our observations in time, also argues against significant variations in the planetary wind. In any case, all of the Wang & Dai (2021b) models that include a stellar wind suggest that the planet should have a trailing tail—which would contaminate the posttransit spectra—so it is difficult to avoid a tail as the cause of the observed variation.

5.2. Modeling the Outflowing Gas from WASP-107b

Because there is no significant pretransit baseline on the night of our January transit observations, we cannot conclusively measure when the excess absorption diminishes entirely from the light curve, and therefore measure the size of an extended tail. However, we can make an estimate, if we assume

that the transit depth at 10830 Å did not change between January and April (which may not necessarily be true because of the reasons discussed above). When the transit depths are matched, as described in Section 4.2, the January transit light curve reaches the unitary baseline at a phase of around 0.0186 (dashed–dotted line in Figure 4). This phase corresponds to an orbital length of 5.0×10^5 km; ~7.0 planet radii, or roughly twice the planetary Roche lobe radius (calculated using the parameters in Table 1 and Equation (2) of Eggleton 1983).

The effect of stellar wind on escaping exoplanet atmospheres has been a topic of considerable interest in recent years (e.g., Stone & Proga 2009; Matsakos et al. 2015; Christie et al. 2016; Villarreal D'Angelo et al. 2018; Carolan et al. 2021). For example, McCann et al. (2019) used hydrodynamical models of escaping atmospheres to study the effects of varying stellar environments—including stellar winds—in the context of Lyα transit observations of irradiated gas giants. Their results, which concerned the bulk loss of atmospheric material, are relevant to WASP-107b, even though we observed metastable helium rather than hydrogen. They showed that with a very weak stellar wind, lost material from a highly irradiated planet forms a low-density torus around the star. This would not impart a significant time-varying signal on observed spectra. On the other hand, the radial force of a strong stellar wind directs the lost material into a dense stream (which is also shaped by the rotational and orbital motion of the planet). It is this radially-directed stream that results in excess blueshifted absorption posttransit. It may therefore be possible to infer the relative strengths of the planetary and stellar winds from observations of posttransit tails like that of WASP-107b (M. MacLeod & A. Oklopčić 2021, in preparation).

In Figure 4 we show the fiducial light-curve model of WASP-107b at 10830 Å from the hydrodynamical simulations of Wang & Dai (2021b), which include stellar wind effects. They used a stellar wind density at WASP-107b's orbital distance of 1.7×10^{-19} g cm^{-3} (about 20 times the solar value) and high-energy fluxes slightly higher than a typical K5 star, and found a mass-loss rate of around 1.02×10^{-9} Earth-masses per year. We did not fit the model to our data, yet the observed posttransit absorption is remarkably similar to that of the simulation, as is the overall shape of the light curve. The model is slightly shallower than the data from 1st contact until midtransit. McCann et al. (2019) show how increasing the stellar wind density can compress the mass-loss flow on the eastern limb of the planet, and thus truncate any pretransit absorption signals. Perhaps these observations might therefore be better explained by a more rarefied stellar wind.

Because our observations provide the only posttransit coverage of WASP-107b at high resolution around 10830 Å so far, it is difficult to search for variability caused by shear instabilities, which is expected to be most dramatic in the pre and posttransit epochs. There is a small amount of pretransit absorption in the light curves of Allart et al. (2019), Kirk et al. (2020), and this work. However, all three data sets are consistent within the 1σ errors when we normalize our light curve as described in Section 4.2. Because we normalized the light curve by matching our data to the Kirk et al. (2020) between the second and third contacts only, our analysis would not be affected by pre or posttransit variability. Finally, our main conclusion—that WASP-107b has a long, posttransit tail—would be unaffected by incorrect light-curve normalization because the normalization would not change the prolonged egress that we observed.

6. Discussion and Conclusions

To summarize, we directly observed excess, posttransit absorption for WASP-107b at 10830 Å, with NIRSPEC on Keck. The most likely cause is a comet-like tail of lost atmospheric material trailing the planet, which is a common feature seen in 3D numerical simulations of escaping exoplanet atmospheres. The posttransit absorption we measured is remarkably similar to the simulations of WASP-107b from Wang & Dai (2021b). Hints of a tail were noted by Kirk et al. (2020), who observed excess absorption during egress; however, they did not have as much posttransit phase coverage as we did. Our transmission spectrum, constructed assuming the nominal "out-of-transit" epochs (i.e., assuming no excess helium absorption in the postegress spectra) is significantly different than the two previously published absorption spectra at 10830 Å, which were constructed using out-of-transit spectra derived from either solely (Kirk et al. 2020) or mostly (Allart et al. 2019) pretransit epochs. We cannot rule out contribution from the contrast effect, i.e., crossing over different active/quiet regions of the star from epoch to epoch. However, WASP-107b's asymmetrical light curve and a deeper and more blueshifted posttransit spectrum (compared to previous observations) point to a tail as the most likely physical cause of the difference.

There are two other exoplanets which show evidence for posttransit tails at 10830 Å: the warm, Saturn-mass WASP-69b (Nortmann et al. 2018) and the hot-Jupiter HD189733b (e.g., Guilluy et al. 2020). The posttransit absorption for HD189733b is of fairly low significance, and therefore Guilluy et al. (2020) do not provide an estimate of its extent. For WASP-69b, Nortmann et al. (2018) measured significant posttransit absorption for at least 20 minutes after fourth contact in two transit observations, and they also observed a blueshift in the 10830 Å lines at that time. They calculated that WASP-69b's tail extends to around 1.7×10^5 km, 2.4 Jupiter radii, or 1.2 times WASP-69b's Roche lobe radius. WASP-69b is a particularly interesting planet to compare to WASP-107b because they both have fairly similar stellar host types (K6/K5, respectively), orbital distances (0.55/0.45 au), and planetary radii (0.95/1.06 Jupiter radii), but quite different masses (0.096/0.26 Jupiter masses). At 5.0×10^5 km, WASP-107b appears to have a much more extended posttransit tail at 10830 Å, which is perhaps unsurprising, since WASP-107b has much deeper overall excess absorption at midtransit (6% versus 3%). Perhaps it is the lower gravitational potential of the planet, which leads to a more extended cloud of material encircling and trailing the planet. In any case, WASP-107b appears to have the most dramatic posttransit tail of any exoplanet observed at 10830 Å so far.

WASP-107b has a nominal planetary transit duration of 2.7 hr, plus a tail that shows excess absorption for around 80 minutes after the nominal egress. A full transit, with pre-egress and a posttail baseline will be necessary to better constrain the size and kinematics of the tail. In order to observe the entire transit from the ground, with ample pre and posttransit baseline, the midtransit time needs to occur close to the middle of a given night. One half night of telescope time, we have shown, is not enough. Because it only transits once every 5.7 days, such events will be rarer for WASP-107b than for typical

hot-Jupiter exoplanets, which usually have shorter orbital periods. A scheduled transit observation lasting 6.5 hr (program ID:1224, PI:Birkmann) with NIRSpec on the James Webb Space Telescope (JWST), which covers 10830 Å, may be long enough to cover the required phases to observe the full tail. The medium resolution of the JWST observations ($R \sim 2700$) will impede detailed characterization of the helium absorption line profile, but the precision of the spectrophotometric light curve will be unmatched. Since WASP-107b remains the planet with the largest absorption depth and signal-to-noise ratio, and now has the largest observed tail at 10830.3 Å, observations of a full transit of the planet and tail will be essential for validating hydrodynamical models and investigating the influence of stellar wind on escaping atmospheres. Finally, we advise caution in selecting spectra to use for the baseline stellar flux for any transmission spectrum, when the spatial extent of the planetary atmosphere is unknown.

We are extremely grateful to Carlos Alvarez and Greg Doppmann for their expert assistance with Keck/NIRSPEC operations, especially during the early postupgrade epoch of our observations, and to Emily Martin for helpful preobservation conversations concerning the upgraded instrument. We thank Trevor David, James Kirk, Ryan Rubenzahl, Michael Zhang, Fei Dai, Heather Knutson, and Romain Allart for helpful discussions. We also thank Lile Wang and Fei Dai for the model light curve.

We thank the expert referee for helpful comments.

A.O. gratefully acknowledges support from the Dutch Research Council NWO Veni grant. J.J.S. is supported by the Heising Simons *51 Pegasi b* postdoctoral fellowship.

The data presented herein were obtained at the W. M. Keck Observatory, which is operated as a scientific partnership among the California Institute of Technology, the University of California, and the National Aeronautics and Space Administration. The Observatory was made possible by the generous financial support of the W. M. Keck Foundation. The authors wish to recognize and acknowledge the very significant cultural role and reverence that the summit of Maunakea has always had within the indigenous Hawaiian community. We were most fortunate to have the opportunity to conduct observations from this mountain.

Facility: Keck:II (NIRSPEC).

Software: SciPy (Virtanen et al. 2020); NumPy (Van Der Walt et al. 2011); matplotlib (Hunter 2007); Astropy (Astropy Collaboration et al. 2013); and iSpec (Blanco-Cuaresma et al. 2014).

ORCID iDs

J. J. Spake https://orcid.org/0000-0002-5547-3775
A. Oklopčić https://orcid.org/0000-0002-9584-6476

References

Allart, R., Bourrier, V., Lovis, C., et al. 2018, Sci, 362, 1384
Allart, R., Bourrier, V., Lovis, C., et al. 2019, A&A, 623, A58
Alonso-Floriano, F. J., Snellen, I. A. G., Czesla, S., et al. 2019, A&A, 629, A110
Anderson, D. R., Collier Cameron, A., Delrez, L., et al. 2017, A&A, 604, A110
Astropy Collaboration, Robitaille, T. P., Tollerud, E. J., et al. 2013, A&A, 558, A33
Bisikalo, D., Kaygorodov, P., Ionov, D., et al. 2013, ApJ, 764, 19
Blanco-Cuaresma, S., Soubiran, C., Jofré, P., & Heiter, U. 2014, in ASI Conf. Ser. 11, International Workshop on Stellar Spectral Libraries, ed. H. P. Singh et al. (Hyderabad: ASI), 85
Bourrier, V., Lecavelier des Etangs, A., Dupuy, H., et al. 2013, A&A, 551, A63
Bourrier, V., Lecavelier des Etangs, A., Ehrenreich, D., Tanaka, Y. A., & Vidotto, A. 2016, A&A, 591, A121
Carolan, S., Vidotto, A. A., Villarreal D'Angelo, C., & Hazra, G. 2021, MNRAS, 500, 3382
Carroll-Nellenback, J., Frank, A., Liu, B., et al. 2017, MNRAS, 466, 2458
Cauley, P. W., Redfield, S., Jensen, A. G., et al. 2015, ApJ, 810, 13
Cauley, P. W., Redfield, S., Jensen, A. G., & Barman, T. 2016, AJ, 152, 20
Cauley, P. W., Kuckein, C., Redfield, S., et al. 2018, AJ, 156, 189
Cegla, H. M., Watson, C. A., Shelyag, S., et al. 2018, ApJ, 866, 55
Christie, D., Arras, P., & Li, Z.-Y. 2016, ApJ, 820, 3
Dai, F., & Winn, J. N. 2017, AJ, 153, 205
Eggleton, P. P. 1983, ApJ, 268, 368
Ehrenreich, D., Bourrier, V., Wheatley, P. J., et al. 2015, Natur, 522, 459
Fossati, L., Haswell, C. A., Froning, C. S., et al. 2010, ApJL, 714, L222
Fulton, B. J., Petigura, E. A., Howard, A. W., et al. 2017, AJ, 154, 109
Ginzburg, S., Schlichting, H. E., & Sari, R. 2018, MNRAS, 476, 759
Guilluy, G., Andretta, V., Borsa, F., et al. 2020, A&A, 639, A49
Hunter, J. D. 2007, CSE, 9, 90
Husser, T. O., Wende-von Berg, S., Dreizler, S., et al. 2013, A&A, 553, A6
Jensen, A. G., Redfield, S., Endl, M., et al. 2012, ApJ, 751, 86
Kasper, D., Bean, J. L., Oklopčić, A., et al. 2020, AJ, 160, 258
Kausch, W., Noll, S., Smette, A., et al. 2015, A&A, 576, A78
Khodachenko, M. L., Shaikhislamov, I. F., Lammer, H., et al. 2019, ApJ, 885, 67
Kim, S., Prato, L., & McLean, I. 2015, REDSPEC: NIRSPEC Data Reduction, Astrophysics Source Code Library, ascl:1507.017
Kirk, J., Alam, M. K., López-Morales, M., & Zeng, L. 2020, AJ, 159, 115
Kulow, J. R., France, K., Linsky, J., & Loyd, R. O. P. 2014, ApJ, 786, 132
Lavie, B., Ehrenreich, D., Bourrier, V., et al. 2017, A&A, 605, L7
Lecavelier Des Etangs, A., Ehrenreich, D., Vidal-Madjar, A., et al. 2010, A&A, 514, A72
Lecavelier des Etangs, A., Bourrier, V., Wheatley, P. J., et al. 2012, A&A, 543, L4
Lopez, E. D., & Fortney, J. J. 2013, ApJ, 776, 2
Mansfield, M., Bean, J. L., Oklopčić, A., et al. 2018, ApJL, 868, L34
Martin, E. C., Fitzgerald, M. P., McLean, I. S., et al. 2018, Proc. SPIE., 10702, 107020A
Matsakos, T., Uribe, A., & Königl, A. 2015, A&A, 578, A6
McCann, J., Murray-Clay, R. A., Kratter, K., & Krumholz, M. R. 2019, ApJ, 873, 89
McCullough, P. R., Crouzet, N., Deming, D., & Madhusudhan, N. 2014, ApJ, 791, 55
McLean, I. S., Becklin, E. E., Bendiksen, O., et al. 1998, Proc. SPIE, 3354, 566
McLean, I. S., Graham, J. R., Becklin, E. E., et al. 2000, Proc. SPIE, 4008, 1048
Ninan, J. P., Stefansson, G., Mahadevan, S., et al. 2020, ApJ, 894, 97
Nortmann, L., Pallé, E., Salz, M., et al. 2018, Sci, 362, 1388
Oklopčić, A. 2019, ApJ, 881, 133
Oklopčić, A., & Hirata, C. M. 2018, ApJL, 855, L11
Owen, J. E., & Wu, Y. 2013, ApJ, 775, 105
Palle, E., Nortmann, L., Casasayas-Barris, N., et al. 2020, A&A, 638, A61
Paragas, K., Vissapragada, S., Knutson, H. A., et al. 2021, ApJL, 909, L70
Piaulet, C., Benneke, B., Rubenzahl, R. A., et al. 2021, AJ, 161, 70
Pont, F., Knutson, H., Gilliland, R. L., Moutou, C., & Charbonneau, D. 2008, MNRAS, 385, 109
Quirrenbach, A., Amado, P. J., Caballero, J. A., et al. 2014, Proc. SPIE, 9147, 91471F
Rackham, B. V., Apai, D., & Giampapa, M. S. 2018, ApJ, 853, 122
Rackham, B. V., Apai, D., & Giampapa, M. S. 2019, AJ, 157, 96
Rubenzahl, R. A., Dai, F., Howard, A. W., et al. 2021, AJ, 161, 119
Salz, M., Czesla, S., Schneider, P. C., et al. 2018, A&A, 620, A97
Seager, S., & Sasselov, D. D. 2000, ApJ, 537, 916
Schneider, J., Rauer, H., Lasota, J. P., Bonazzola, S., & Chassefiere, E. 1998, in ASP Conf. Ser. 134, Brown Dwarfs and Extrasolar Planets, ed. R. Rebolo et al. (San Francisco, CA: ASP), 241
Shaikhislamov, I. F., Khodachenko, M. L., Lammer, H., et al. 2021, MNRAS, 500, 1404
Sing, D. K., Lavvas, P., Ballester, G. E., et al. 2019, AJ, 158, 91
Sing, D. K., Pont, F., Aigrain, S., et al. 2011, MNRAS, 416, 1443
Smette, A., Sana, H., Noll, S., et al. 2015, A&A, 576, A77
Spake, J. J., Sing, D. K., Evans, T. M., et al. 2018, Natur, 557, 68

Stone, J. M., & Proga, D. 2009, ApJ, 694, 205
Van Der Walt, S., Colbert, S. C., & Varoquaux, G. 2011, CSE, 13, 22
Vidal-Madjar, A., Dsert, J.-M., Lecavelier des Etangs, A., et al. 2004, ApJ, 604, L69
Vidal-Madjar, A., Huitson, C. M., Bourrier, V., et al. 2013, A&A, 560, A54
Vidal-Madjar, A., Lecavelier des Etangs, A., Désert, J.-M., et al. 2003, Natur, 422, 143
Villarreal D'Angelo, C., Esquivel, A., Schneiter, M., & Sgró, M. A. 2018, MNRAS, 479, 3115
Virtanen, P., Gommers, R., Oliphant, T. E., et al. 2020, NatMe, 17, 261
Vissapragada, S., Knutson, H. A., Jovanovic, N., et al. 2020, AJ, 159, 278
Wang, L., & Dai, F. 2021a, ApJ, 914, 98
Wang, L., & Dai, F. 2021b, ApJ, 914, 99
Yan, F., & Henning, T. 2018, NatAs, 2, 714
Zhang, M., Knutson, H. A., Wang, L., et al. 2021, AJ, 161, 181